High-Efficiency Polymer Solar Cells Enhanced by Solvent Treatment

Huiqiong Zhou, Yuan Zhang, Jason Seifter, Samuel D. Collins, Chan Luo, Guillermo C. Bazan, Thuc-Quyen Nguyen, and Alan J. Heeger*

Polymer solar cells (PSC) using polymer-fullerene bulk heterojunctions (BHJ) have been extensively studied due to their promising advantages including low-cost manufacturability. They are mechanically robust and flexible.[1–3] Moreover, the materials from which they are made are readily available. New narrow bandgap materials with suitable energy alignment[4–7] and device optimization by utilizing different device structures[8–13] or controlling morphology of active layers[14,15] are successful strategies to improve the power conversion efficiencies (PCEs). Recently, significant efforts have been dedicated to the interface engineering of polymer solar cells.[16–18] Interface properties which are also critical to the device performance can be dramatically changed by incorporating a functional interfacial layer between active layer and metal electrode.[11,13,19–26] Many interfacial materials, such as metal oxides,[5,10,12,27] self-assembled monolayers (SAMs)[28,29] and conjugated polyelectrolytes (CPEs),[8,21–26] have successfully enhanced PCEs of solar cells fabricated through solution processing.

More interestingly, several independent groups have found that the device performance could be considerably enhanced by treatment with polar solvents that are commonly used in interface engineering through solution processing in organic photovoltaics before deposition of metal electrodes.[30–33] The positive effects of solvents on device performance are thought to optimize the phase separation in BHJ active layers[31,32] or probably even to change the interface between the BHJ active layer and the poly(3,4-ethylenedioxythiophene) poly(styrenesulfonate) (PEDOT:PSS) layer underneath.[30] However, these interesting phenomena and attractive effects originating from simple solvents treatment are poorly understood.

In this study, we focus on understanding the effect of solvent treatment on the device physics of polymer solar cells. Methanol was chosen as typical solvent because it has been widely used in surface engineering to incorporate interlayers in photovoltaics.[20,21,24–27] Polymer:fullerence BHJ solar cells based on [6,6]-phenyl C71-butyric acid methyl ester ($PC_{70}BM$) and a low-bandgap donor material thieno[3,4-b]-thiophene/benzodithiophene (PTB7) (the molecular structure shown in the insert in **Figure 1**b)[4,8,12,25] show simultaneous enhancement in short-circuit current (J_{sc}), open-circuit voltage (V_{oc}), and fill factor (FF), which leads to significant improvement of PCEs from 7.1% to 7.9% using Ca/Al as cathodes after methanol treatment of the active layer, while from 5.4% to 7.2% using Al as cathodes.

Figure 1a shows the current density versus voltage ($J–V$) characteristics of the best PTB7 PSCs with and without methanol treatment under 1000 W m^{-2} air mass 1.5 global (AM 1.5 G) illumination. A high PCE of 7.20 ± 0.11% was achieved in optimized devices using Al cathodes with methanol treatment of the active layer, compared with a PCE a 5.44 ± 0.15% obtained for the control devices. Methanol treatment leads to a significant 30% enhancement in PCE with a simultaneous improvement in V_{oc} (0.72 ± 0.01 V to 0.75 ± 0.01 V), J_{sc} (11.47 ± 0.21 mA cm^{-2} to 13.92 ± 0.21 mA cm^{-2}) and FF (64 ± 1% to 68 ± 1%). When Ca/Al is used as the cathode (shown in insert of Figure 1a), PCE increased from 7.10 ± 0.10% to 7.94 ± 0.10% after methanol treatment with enhancement in V_{oc} (0.73 ± 0.01 V to 0.76 ± 0.01 V), J_{sc} (15.24 ± 0.13 mA cm^{-2} to 15.46 ± 0.13 mA cm^{-2}) and FF (63 ± 1% to 68 ± 1%). It's interesting to note that when Al is replaced by Ca/Al as cathode, a smaller enhancement in PCE was observed yet the overall performance is higher. This phenomenon can be attributed to the contact of LUMO of $PC_{70}BM$ with Ca/Al that is more ohmic than with using Al due to interfacial doping by Ca, such that voltage losses due to interfacial band bending can be effectively suppressed.

Under illumination, the device with methanol treatment and Al cathode shows a V_{oc} of 0.75 V, which is higher than the control devices of 0.72 V. In the dark, the device with methanol treatment exhibits a turn-on voltage of 0.80 V while it is 0.70 V for the control device (Figure 1b), which indicates that the built-in voltage (V_{bi}) (here considered as flat-band condition) of the device increases around 100 mV after methanol treatment. V_{bi} increases by a similar amount when using Ca/Al as cathode. The V_{bi}, which influences the internal electric field in polymer BHJ solar cells, is an important parameter and gives the upper limit for the V_{oc} provided that the work function difference of electrodes is larger than the donor HOMO-acceptor LUMO offset of the BHJ.[34,35] Thus the increase of V_{bi} may be responsible for the increase in V_{oc} in the devices after methanol treatment.

To study the modification of solvent treatment on the PTB7:$PC_{70}BM$ surface, we directly examine the surface potential by Kelvin probe force microscopy (KPFM), the surface morphology by atomic force microscopy (AFM) and the surface

Dr. H. Zhou,[+] Dr. Y. Zhang,[+] J. Seifter, S. Collins,
Dr. C. Luo, Prof. G. C. Bazan, Prof. T.-Q. Nguyen,
Prof. A. J. Heeger
Center for Polymers and Organic Solids
University of California
Santa Barbara, CA 93106, USA
E-mail: ajhe@physics.ucsb.edu
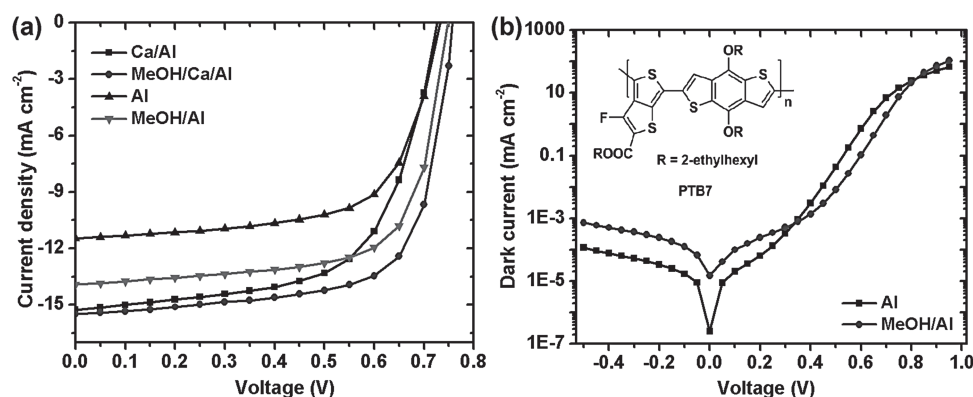[+]Dr. H. Zhou and Dr. Y. Zhang contributed equally to this work.

Figure 1. The effect of methanol treatment on PTB7:PC$_{70}$BM solar cell performance. a) Current density versus voltage (J–V) characteristics for Ca/Al devices without (squares, 7.10%) and with (circles, 7.94%) methanol treatment, for Al devices without (up-triangles, 5.44%) and with (down-triangles, 7.20%) methanol treatment. All of the devices were measured under 1000 W m^{-2} AM 1.5 G illumination. b) J–V characteristics of Al devices with (circles) and without methanol treatment (squares) in the dark. The inset shows the molecular structure of PTB7.

composition by X-ray photoelectron spectroscopy (XPS). KPFM measures two-dimensional distributions of contact potential difference (CPD) between the tip and the sample with a resolution in the nanometer range.[36] KPFM measurements of the surface of the active layer show a 101 ± 19 mV shift in average surface potential occurring after methanol treatment (**Figure 2**a,b), which suggests that at the metal/organic interface, the vacuum level (VL) of the cathode is correspondingly elevated 101 ± 19 mV simply by methanol treatment. A similar increase in surface potential has been observed in organic light-emitting diode devices utilizing solvent treatment.[33] The surface potential is an extremely sensitive indicator of surface condition and can be affected by electronic states on the surface including surface charge density or surface traps, surface reconstruction, and chemical composition, etc.[36,37] Figure 2c,d show the surface morphology of PTB7:PC$_{70}$BM films before and after methanol treatment examined by AFM. The pristine PTB7:PC$_{70}$BM film exhibits a homogeneous, relatively rough surface with a root mean square (rms) roughness of 5.6 nm. Methanol treatment causes no obvious change on morphology and film roughness. There is also no observable change in the film thickness verified by profilometry and no obvious change in the absorption spectrum of PTB7:PC$_{70}$BM films (Supporting Information, Figure S1) after methanol treatment. These observations indicate no evident reconstruction of the surface of PTB7:PC$_{70}$BM blends after methanol treatment. XPS results (Supporting Information, Figure S2) show similar elemental composition on PTB7:PC$_{70}$BM surfaces with and without methanol treatment, which indicates that the effect of methanol treatment on surface chemical composition of PTB7:PC$_{70}$BM films is negligible. In our case, the increase of surface potential as measured by KPFM

might originate from the charge of surface electronic states including the diminishment of surface traps or variation of charge density after methanol treatment.

In order to further explore the effect of methanol treatment on surface electronic states of PTB7:PC$_{70}$BM active layers, we performed capacitance (C)–voltage (V) measurements[20,38] and AC impedance measurements[12,39–42] of PTB7:PC$_{70}$BM solar cells with and without methanol treatment. The upper-limit of doping density (N) can be determined by the slope of Mott–Schottky plot using $N = -2(dC(x)^2/dV)^{-1}/q\varepsilon_0\varepsilon_r A^2$, with q for the elementary charge, ε_0 for the dielectric constant of vacuum,
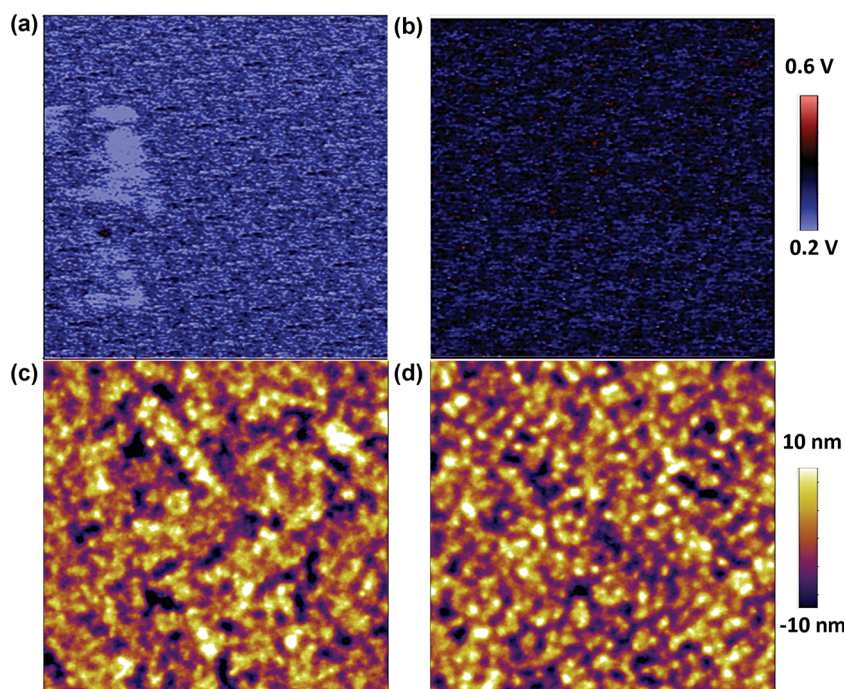

Figure 2. The effect of methanol treatment on surface potential for PTB7:PC$_{70}$BM solar cell. a,b) Contact potential difference (CPD) images of the active layer without (a) and with methanol treatment (b) obtained from KPFM. c,d) Surface topographic AFM images (size: 5 μm × 5 μm) without (c) and with methanol treatment (d).
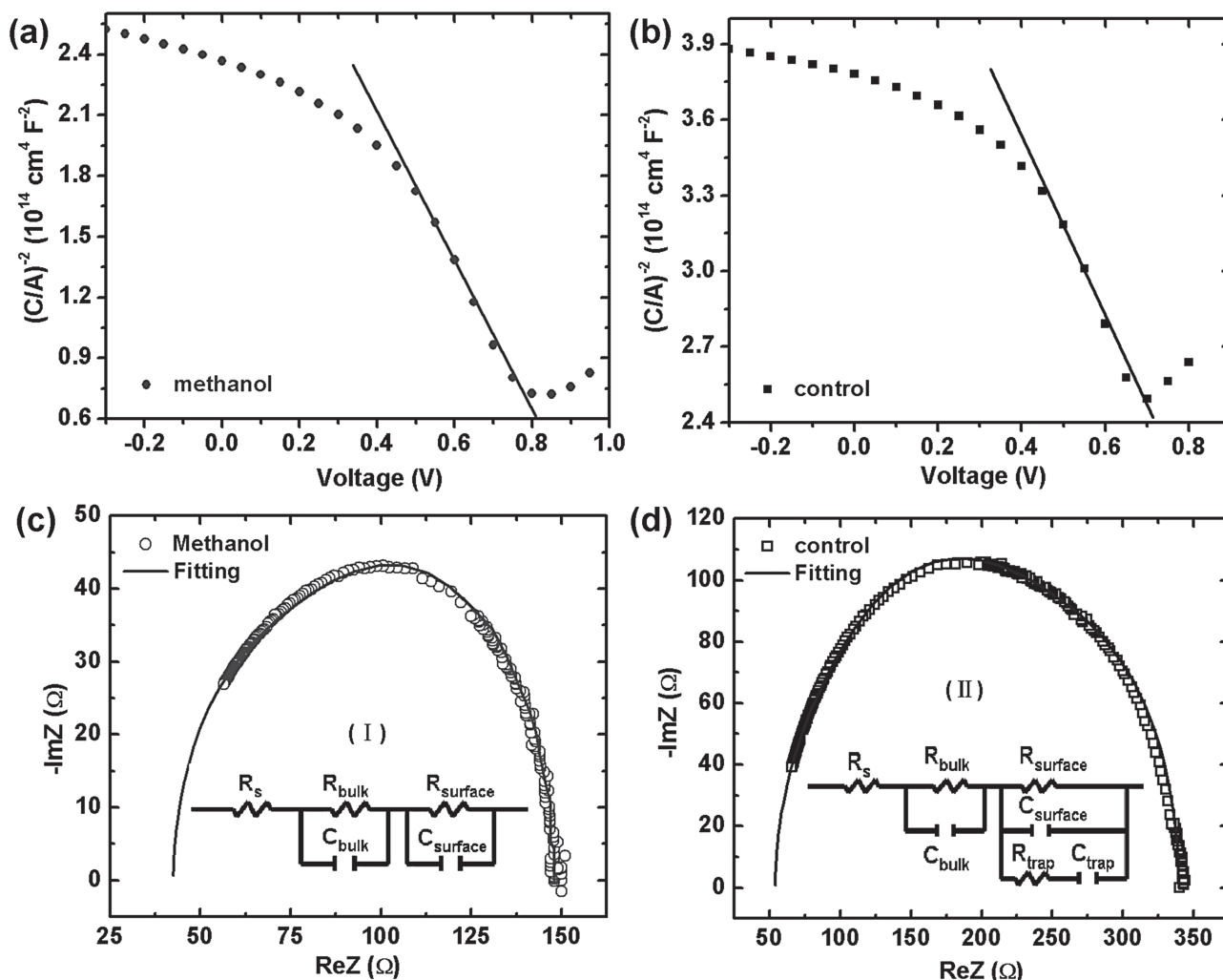
Figure 3. Impedance spectra analysis for the effect of methanol treatment on PTB7:PC$_{70}$BM solar cell. a,b) $(C/A)^{-2}$ versus applied bias voltage with (a) and without (b) methanol treatment. The solid lines correspond to Mott–Schottky plot. c,d) Niquist plots for PTB7:PC$_{70}$BM solar cells with (c) and without (d) methanol treatment. The data are fitted by equivalent circuit models I and II separately.

and ε_r for the relative dielectric constant of the semiconductor (assuming ε_r of 3.5).[43] We estimated the values of V_{bi} by the voltage corresponding to the maximal of capacitance which equals the flat-band condition,[44,45] due to the lack of well-defined Schottky contacts in this case. Our analysis methods provide an appropriate comparison of the differences of V_{bi} and N in the devices induced by methanol treatment. $C–V$ characteristics shown in **Figure 3**a,b were attained by applying a low AC perturbation signal with fixed frequency and sweeping the DC bias. For pristine PTB7:PC$_{70}$BM solar cells (Figure 3a), we obtain a V_{bi} of 0.72 ± 0.02 V and the maximum value of N is (5.23 ± 1.12) × 10^{16} cm^{-3}, which roughly defines the upper limit for this device. After methanol treatment (Figure 3b), the V_{bi} is 0.83 ± 0.02 V and the maximum value of N increases to around (8.80 ± 1.35) × 10^{16} cm^{-3}. Since there is no substantial influence on the thickness of active layers, this 110 ± 20 mV increase of V_{bi} which matches the value measured by KPFM is attributed to the methanol treatment. The increase of N after methanol treatment may lead to an increase of the surface charge density

and thereby increase the surface potential shown by KPFM measurement.

Figure 3c,d show Nyquist plots of impedance measurement of PTB7:PC$_{70}$BM devices with and without methanol treatment for frequencies from 500 Hz to 1 MHz. The data were fit by using equivalent circuit modeling (ECM) with detailed circuits depicted by inserted graphs. For the device treated with methanol, an ECM comprised with a double RC in parallel connection (Model I) was applied, where the two capacitors stand for the depletion ($C_{surface}$) and bulk capacitance (C_{bulk}), respectively. As a result the ECM yields satisfactory agreement with the measurements. In contrast Model I described in the inset of Figure 3c cannot be satisfactorily applied for the control device (Supporting Information, Figure S3b). We suspect there are surface traps existing on the surface of active layers in control samples and thus add extra RC in series connected in parallel with the depletion capacitance to improve the data modeling (Figure 3d, Model II). This extra RC component (C_{trap}) attributed to the surface traps which has been previously applied in

other BHJ systems.[39] We found that using the additional surface traps correlated RC components is essential for modeling the impedance of the control device while not necessary for the methanol-treated device (Supporting Information, Figure S3a). These observations indicate that surface traps may become less significant upon solvent passivation. Detailed mechanisms are worthy of further investigation and are still in progress. The passivation of surface traps is consistent with the observation of charge carrier density increase as mentioned above. In addition, the series resistance (R_s) can be obtained from the intercept on ReZ axis at high frequencies (left part) in Nyquist plots.[42] After methanol treatment, R_s is reduced from 2.61 Ω cm^2 to 1.84 Ω cm^2 in PTB7:PC$_{70}$BM solar cells in agreement with the observed improvement in J_{sc} and FF.

Based on our results, the increase of V_{oc} primarily can be ascribed to enhanced V_{bi} in PTB7:PC$_{70}$BM devices after methanol treatment, as confirmed by KPFM measurement and $C-V$ measurement. For an enhancement of V_{bi} of 100 mV, the increase in V_{oc} only amounts to 20–40 mV. This smaller enhancement in V_{oc} may result from Fermi level pinning between the cathode and the acceptor PC$_{70}$BM in the active layer.[34] In addition to the increase of V_{oc}, improvements in J_{sc} and FF were also observed upon methanol treatment. In general, J_{sc} and FF would be intimately affected by R_s, charge-transport properties, charge extraction and charge recombination.

The effects of methanol treatment on charge-transport properties were investigated by examining the carrier mobilities of PTB7:PC$_{70}$BM using single-carrier diodes and the space-charge limited current (SCLC) model. The current in the PTB7:PC$_{70}$BM blend combines contributions of both the electron and hole; therefore, one needs to facilitate the injection of one type of the carriers and suppress the other by choosing appropriate electrodes in order to fabricate electron-only or hole-only devices[46–48] (details can be found in Experimental Section). The current-voltage curve was fit using the Mott–Gurney law (Supporting Information, Figure S4), $J = 9\varepsilon_r\varepsilon_0\mu(V - V_{bi})^2/8L^3$, where $\varepsilon_r\varepsilon_0$ is the dielectric permittivity of the active layer, μ is the mobility, and L is the thickness of active layer. In pristine PTB7:PC$_{70}$BM devices, the hole mobility of 5.4×10^{-5} cm^2 V^{-1} s^{-1} is nearly two orders of magnitude lower than the electron mobility of 2.1×10^{-3} cm^2 V^{-1} s^{-1}. After methanol treatment, the hole mobility increases to 1.6×10^{-4} cm^2 V^{-1} s^{-1}, while the electron mobility remains unchanged. Thus, more balanced charge transport in the devices can be achieved, which may increase the FF in the devices by restricting the build-up of space charges, and hence, reducing charge recombination.

In order to study the influence of the methanol treatment on the extraction and recombination of charge carriers in PTB7:PC$_{70}$BM devices, internal field dependent transient photoconductivity measurements were performed. From Figure S5a,b in the Supporting Information, it can be seen that a transient photocurrent trace is characterized by an initial, voltage-dependent sweepout of mobile carriers, followed by a long, bias-insensitive photocurrent tail, which is a result of the slow recombination and detrapping of trapped charges from a distribution of subgap energy states.[49] By integrating these current traces (Supporting Information, Figure S5c), the total extracted charge can be obtained as a function of applied bias against the built-in voltage. As

the internal field is reduced for each device, fewer charges are extracted, as the longer transit time allows for greater recombination.[50] **Figure 4**a shows the charge extraction of both devices at J_{sc} condition where the internal field equals the V_{bi}. The faster decay kinetics after methanol treatment indicates faster charge extraction of the mobile carriers, which may result from either a higher V_{bi} or increased carrier mobility. This difference vanishes once an external voltage of 100 mV is applied to the methanol-treated cell, which compensates the V_{bi} difference, and equalizes the internal fields of the two devices (Figure 4b), illustrating that it is the enhanced V_{bi} which results in improved sweepout of mobile carriers. This observation holds at other applied voltages as well, as long as the total internal fields of the devices are kept the same. Interestingly, even when the internal fields of the devices are equalized, the methanol treated sample still extracts significantly more total charge than the untreated solar cell (shown in Supporting Information, Figure S5c). Examination of the long tail of the photoconductivity traces, where the photocurrent is dominated by subgap trap states, helps to understand this increased charge extraction. Figure 4c shows the transient photoconductivity curves of the two solar cells near the maximum power point, with the samples asymmetrically biased to equalize the internal fields of the devices. The short timescale sweepout characteristics are very similar, evidenced by the fact that there is no significant difference in total extracted charge between the devices for the first 700 nanoseconds (shown in the inset of Figure 4c). In order to decouple the current contribution due to the mobile carrier sweep out from that of the trap-dominated tails, the tails were fitted beyond the sweep out time, and then extrapolated back to determine their zero time values. The tails were then integrated, and the methanol sample was found to yield 26% more charges from the long-lived tail than the control device. When carriers fall into traps, the two possible eventual fates of these charges are recombination or emission and eventual collection. As recombination rates go up, the current trace will decay faster, and the integrated extracted charge will decrease. As emission and collection rates go up, the measured current will stay higher. The control sample has a noticeably steeper decay in the tail than the methanol treated cell, which suggests that the methanol treatment lowers the recombination rate, increasing the carrier lifetime, and/or decreases the average energy of the existing trap states, allowing for a greater emission and collection rate. Transient photoconductivity measurements alone cannot differentiate whether this is a surface or bulk effect, but when combined with the previous impedance analysis, we attribute this effect to the passivation of surface traps in the devices. When this effect is further accompanied by the increased internal field to sweep out the mobile carriers efficiently, a significant improvement in device performance can be observed.

Studies of impedance measurements, single-carrier devices, and transient photoconductivity confirm that methanol treatment induces a passivation of surface traps, a lowered series resistance, an increased hole mobility, an accelerated and augmented charge extraction and a reduced charge recombination due to enlarged V_{bi} and/or decrease of trap density. All these improvements give rise to the observed enhancement of the J_{sc} and FF.

In conclusion, high-efficiency polymer solar cells (PTB7:PC$_{70}$BM) with PCE of 7.9% was achieved by methanol treatment. The effects of methanol treatment on the
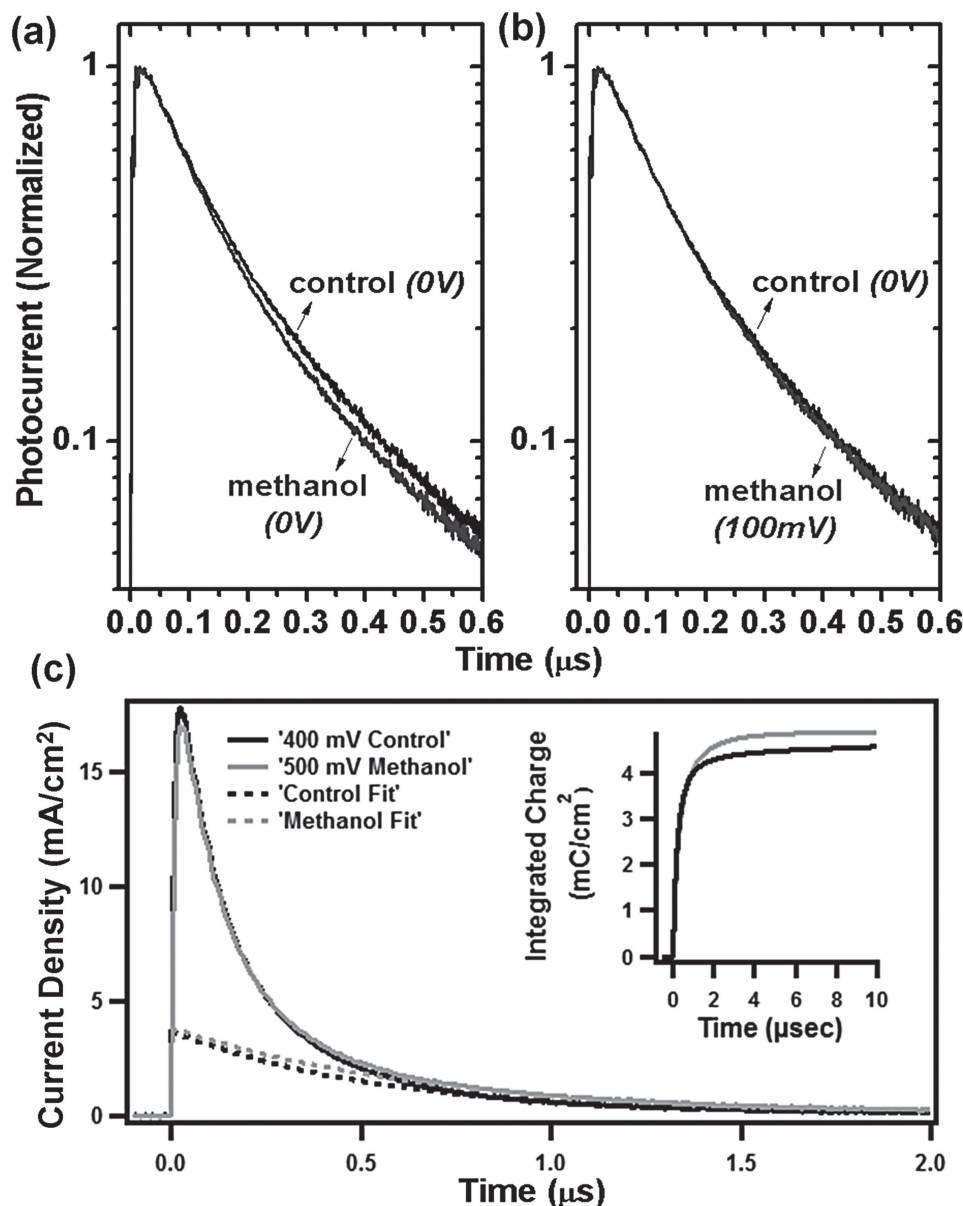
Materials
Views
www.MaterialsViews.com

ADVANCED
MATERIALS
www.advmat.de

COMMUNICATION

Figure 4. Transient photocurrent (normalized) of PTB7:PC$_{70}$BM solar cells with and without methanol treatment: a) Both cells at J_{sc} condition; b) 100 mV compensated bias on methanol-treated cells and 0 V bias on control cells. c) Transient photocurrent (un-normalized) of PTB7:PC$_{70}$BM with and without methanol treatment near the maximum power point; the photocurrent tails were fitted and back-extrapolated. The inset shows the integrated photocurrent as a function of time for these two cells.

enhancement of device performance are shown to originate from an increase in built-in voltage across the device due to passivation of surface traps and a correspondingly increase of surface charge density. Combined with decreased series resistance and increased mobilities, accelerated and enlarged charge extraction and reduced charge recombination were obtained. All these effects induce a simultaneous enhancement in the open-circuit voltage, short-circuit current density, and fill factor of device performance after methanol treatment. This result provides deeper insight to understand the mechanism of surface engineering by solution processing which cannot exclude the effect of solvents. Furthermore, this strategy obviates laborious synthesis

of interlayer materials and utilizes environmental green solvent, which may offer a simple and efficient method to improve PCEs of polymer BHJ solar cells in laboratory study or industry fabrication.

Experimental Section

Device Fabrication: PTB7 was purchased from 1-Material Chemscitech Inc. (St-Laurent, Quebec, Canada) and used as received. The device structure was indium tin oxide (ITO)/PEDOT:PSS/PTB7: PC$_{70}$BM/(Ca)/ Al. A thin layer (≈30 nm) of PEDOT:PSS (Baytron PVP Al 4083) was spin-

coated onto a cleaned ITO surface and annealed in air at 140 °C for 10 min. Then, blend films of PTB7:PC$_{70}$BM were cast from a solution with PTB7:PC$_{70}$BM ratio of 1:1.5 (PTB7 concentration of 10 mg/mL) in chlorobenzene/1,8-diiodoctane (97:3 vol%) mixed solvent at 1000 rpm for 2 min. After dried in vacuum, methanol treatment was carried out by spin-coating methanol solvent on the top of active layers at 2500 rpm for 40 s. The devices were completed after deposition of 100 nm Al or 20 nm Ca/100 nm Al as cathode (4.5 mm^2). Devices were encapsulated for testing in air with a UV-curable epoxy and covered with a glass slide.

Characterization and Measurement: Current density–voltage (*J–V*) characteristics of the devices were measured using a Keithley 236 Source Measure Unit. Solar cell performance used a Newport Air Mass 1.5 Global (AM 1.5G) full spectrum solar simulator with an irradiation intensity of 100 mW cm^{-2}. The 100 mW cm^{-2} spectrum of incident light was spectrum and intensity matched with an Ocean Optics USB4000 spectrometer calibration standard lamp with NIST-traceable calibration from 350–1000 nm. External quantum efficiency (EQE) spectra were measured using a 75 W Xe lamp, Newport monochromator, Newport optical chopper, and a Stanford Research Systems lock-in amplifier. Power-density calibration was done by National Institute of Standards and Technology traceable silicon photodiode.

The surface potential of active layer surfaces was measured by scanning Kelvin probe microscopy (SKPM) in frequency modulation mode, using a single platinum-coated tip with a resonant frequency of 289 kHz in N$_2$ atmosphere. SKPM experiments were implemented using custom code provided by the Ginger Lab for Igor Pro and the Asylum Research XOP. The surface morphology was observed with an atomic force microscope (Bruker Nano; D3100) and a scanning electron microscope (FEI Sirion XL 30).

The XPS measurement was performed using Kratos Ultra spectrometer equipped with monochromatized Al K$_\alpha$ (1486.6 eV) excitation. The capacitance-voltage measurement and the AC impedance measurements were conducted using an Agilent 4192A impedance analyzer. The capacitance-voltage measurements were recorded at a frequency of 100 kHz and a AC bias of 25 mV. The AC impedance measurements were done in *Z-θ* mode for a varying frequency (*f*), from 500 Hz to 1 MHz, with an AC drive bias of 25 mV. A constant DC bias equivalent to the open-circuit voltage of the solar cell device was applied, superimposed on the AC bias. SCLC measurements for PTB7:PC$_{70}$BM devices were explored in configuration of: a) ITO/PEDOT:PSS/active layer/Au for hole-only device; and b) ITO/Al/active layer/Ca/Al for electron-only device. Three different thicknesses of 240 nm, 150 nm and 100 nm were utilized.

For transient photoconductivity measurements, PTB7:PCBM solar cells were excited with a nitrogen-pumped dye laser (Stanford Research Systems NL100 nitrogen laser) pumping a cuvette of Rhodamine 6G laser dye. The pulses were emitted with a duration of ≈5 nsec, a repetition rate of *T* = 1 Hz, a wavelength of *λ* = 590 nm, and an energy of 1.3 nJ per pulse as measured by a Coherent J-10Si-LE Quantum EnergyMax Sensor. The current traces were recorded on a Tektronix DPO3034 digital oscilloscope by measuring the voltage drop over a 5 ohm sensor resistor in series with the solar cell. DC voltage was applied to the solar cell with an MRF544 bipolar junction transistor in common collector amplifier configuration. Typical traces are an average of roughly 250 pulses, all with energy of ±2%.

Supporting Information

Supporting Information is available from the Wiley Online Library or from the author.

Acknowledgements

[1] G. Yu, J. Gao, J. C. Hummelen, F. Wudl, A. J. Heeger, *Science* **1995**, *270*, 1789.

[2] B. C. Thompson, J. M. J. Frechet, *Angew. Chem. Int. Ed.* **2008**, *47*, 58.

[3] C. J. Brabec, S. Gowrisanker, J. J. M. Halls, D. Laird, S. J. Jia, S. P. Williams, *Adv. Mater.* **2010**, *22*, 3839.

[4] Y. Y. Liang, Z. Xu, J. B. Xia, S. T. Tsai, Y. Wu, G. Li, C. Ray, L. P. Yu, *Adv. Mater.* **2010**, *22*, E135.

[5] S. H. Park, A. Roy, S. Beaupre, S. Cho, N. Coates, J. S. Moon, D. Moses, M. Leclerc, K. Lee, A. J. Heeger, *Nat. Photonics* **2009**, *3*, 297.

[6] B. Carsten, F. He, H. J. Son, T. Xu, L. P. Yu, *Chem. Rev.* **2011**, *111*, 1493.

[7] Y. J. Cheng, S. H. Yang, C. S. Hsu, *Chem. Rev.* **2009**, *109*, 5868.

[8] Z. He, C. Zhong, S. Su, M. Xu, H. Wu, Y. Cao, *Nat. Photonics* **2012**, *6*, 593.

[9] C. E. Small, S. Chen, J. Subbiah, C. M. Amb, S.-W. Tsang, T.-H. Lai, J. R. Reynolds, F. So, *Nat. Photonics* **2012**, *6*, 115.

[10] Y. M. Sun, J. H. Seo, C. J. Takacs, J. Seifter, A. J. Heeger, *Adv. Mater.* **2011**, *23*, 1679.

[11] Z. Tang, L. M. Andersson, Z. George, K. Vandewal, K. Tvingstedt, P. Heriksson, R. Kroon, M. R. Andersson, O. Inganas, *Adv. Mater.* **2012**, *24*, 554.

[12] J. You, C.-C. Chen, L. Dou, S. Murase, H.-S. Duan, S. Hawks, T. Xu, H. J. Son, L. Yu, G. Li, Y. Yang, *Adv. Mater.* **2012**, *24*, 5267.

[13] H. Kang, S. Hong, J. Lee, K. Lee, *Adv. Mater.* **2012**, *24*, 3005.

[14] J. Jo, S. I. Na, S. S. Kim, T. W. Lee, Y. Chung, S. J. Kang, D. Vak, D. Y. Kim, *Adv. Funct. Mater.* **2009**, *19*, 2398.

[15] J. Peet, J. Y. Kim, N. E. Coates, W. L. Ma, D. Moses, A. J. Heeger, G. C. Bazan, *Nat. Mater.* **2007**, *6*, 497.

[16] L. M. Chen, Z. Xu, Z. R. Hong, Y. Yang, *J. Mater. Chem.* **2010**, *20*, 2575.

[17] R. Steim, F. R. Kogler, C. J. Brabec, *J. Mater. Chem.* **2010**, *20*, 2499.

[18] H. Ma, H. L. Yip, F. Huang, A. K. Y. Jen, *Adv. Funct. Mater.* **2010**, *20*, 1371.

[19] Y. Zhang, P. Zalar, C. Kim, S. Collins, G. C. Bazan, T.-Q. Nguyen, *Adv. Mater.* **2012**, *24*, 4255.

[20] K. M. O'Malley, C. Z. Li, H. L. Yip, A. K. Y. Jen, *Adv. Energy Mater.* **2012**, *2*, 82.

[21] Y.-M. Chang, R. Zhu, E. Richard, C.-C. Chen, G. Li, Y. Yang, *Adv. Funct. Mater.* **2012**, *22*, 3284.

[22] X. Guan, K. Zhang, F. Huang, G. C. Bazan, Y. Cao, *Adv. Funct. Mater.* **2012**, *22*, 2846.

[23] H. Choi, J. S. Park, E. Jeong, G. H. Kim, B. R. Lee, S. O. Kim, M. H. Song, H. Y. Woo, J. Y. Kim, *Adv. Mater.* **2011**, *23*, 2759.

[24] Z. C. He, C. Zhang, X. F. Xu, L. J. Zhang, L. Huang, J. W. Chen, H. B. Wu, Y. Cao, *Adv. Mater.* **2011**, *23*, 3086.

[25] Z. C. He, C. M. Zhong, X. Huang, W. Y. Wong, H. B. Wu, L. W. Chen, S. J. Su, Y. Cao, *Adv. Mater.* **2011**, *23*, 4636.

[26] J. H. Seo, A. Gutacker, Y. M. Sun, H. B. Wu, F. Huang, Y. Cao, U. Scherf, A. J. Heeger, G. C. Bazan, *J. Am. Chem. Soc.* **2011**, *133*, 8416.

[27] J. Y. Kim, S. H. Kim, H. H. Lee, K. Lee, W. L. Ma, X. Gong, A. J. Heeger, *Adv. Mater.* **2006**, *18*, 572.

[28] H. L. Yip, S. K. Hau, N. S. Baek, H. Ma, A. K. Y. Jen, *Adv. Mater.* **2008**, *20*, 2376.

[29] C. Goh, S. R. Scully, M. D. McGehee, *J. Appl. Phys.* **2007**, 101.

[30] X. Liu, W. Wen, G. C. Bazan, *Adv. Mater.* **2012**, *24*, 4505.

[31] H. Li, H. W. Tang, L. G. Li, W. T. Xu, X. L. Zhao, X. N. Yang, *J. Mater. Chem.* **2011**, *21*, 6563.

[32] S. Nam, J. Jang, H. Cha, J. Hwang, T. K. An, S. Park, C. E. Park, *J. Mater. Chem.* **2012**, *22*, 5543.

[33] Q. Wang, Y. Zhou, H. Zheng, J. Shi, C. Z. Li, C. M. Q. Su, L. Wang, C. Luo, D. G. Hu, J. Pei, J. Wang, J. B. Peng, Y. Cao, *Org. Electron.* **2011**, *12*, 1858.

[34] C. J. Brabec, A. Cravino, D. Meissner, N. S. Sariciftci, T. Fromherz, M. T. Rispens, L. Sanchez, J. C. Hummelen, *Adv. Funct. Mater.* **2001**, *11*, 374.

[35] H. Y. Chen, J. H. Hou, S. Q. Zhang, Y. Y. Liang, G. W. Yang, Y. Yang, L. P. Yu, Y. Wu, G. Li, *Nat. Photonics* **2009**, *3*, 649.

[36] L. S. C. Pingree, O. G. Reid, D. S. Ginger, *Adv. Mater.* **2009**, *21*, 19.

[37] M. Nonnenmacher, M. P. Oboyle, H. K. Wickramasinghe, *Appl. Phys. Lett.* **1991**, *58*, 2921.

[38] P. P. Boix, G. Garcia-Belmonte, U. Munecas, M. Neophytou, C. Waldauf, R. Pacios, *Appl. Phys. Lett.* **2009**, 95.

[39] W. L. Leong, S. R. Cowan, A. J. Heeger, *Adv. Energy Mater.* **2011**, *1*, 517.

[40] Y. Zhang, X. D. Dang, C. Kim, T. Q. Nguyen, *Adv. Energy Mater.* **2011**, *1*, 610.

[41] J. S. Kim, W. S. Chung, K. Kim, D. Y. Kim, K. J. Paeng, S. M. Jo, S. Y. Jang, *Adv. Funct. Mater.* **2010**, *20*, 3538.

[42] T. Kuwabara, Y. Kawahara, T. Yamaguchi, K. Takahashi, *ACS Appl. Mater. Interfaces* **2009**, *1*, 2107.

[43] P. W. M. Blom, V. D. Mihailetchi, L. J. A. Koster, D. E. Markov, *Adv. Mater.* **2007**, *19*, 1551.

[44] S. Nowy, R. Wei, J. Wagner, J. A. Weber, W. Brutting, *Proc. SPIE - Int. Soc. Opt. Eng.* **2009**, *7415*, 74150G1.

[45] K. Harada, A. G. Werner, M. Pfeiffer, C. J. Bloom, C. M. Elliott, K. Leo, *Proc. SPIE - Int. Soc. Opt. Eng.* **2004**, *5464*, 1.

[46] V. D. Mihailetchi, L. J. A. Koster, P. W. M. Blom, C. Melzer, B. de Boer, J. K. J. van Duren, R. A. J. Janssen, *Adv. Funct. Mater.* **2005**, *15*, 795.

[47] Y. Zhang, P. W. M. Blom, *Appl. Phys. Lett.* **2010**, 97.

[48] Y. Zhang, P. W. M. Blom, *Appl. Phys. Lett.* **2011**, 98.

[49] C. G. Shuttle, N. D. Treat, J. D. Douglas, J. M. J. Frechet, M. L. Chabinyc, *Adv. Energy Mater.* **2012**, *2*, 111.

[50] R. A. Street, K. W. Song, J. E. Northrup, S. Cowan, *Phys. Rev. B* **2011**, 83.